HHS Public Access

Author manuscript

IEEE ASME Trans Mechatron. Author manuscript; available in PMC 2021 June 01.

Published in final edited form as:

IEEE ASME Trans Mechatron. 2020 June ; 25(3): 1432–1443. doi:10.1109/tmech.2020.2976897.

Mechatronic Design of a Two-Arm Concentric Tube Robot System for Rigid Neuroendoscopy

Margaret F. Rox* **[Student Member, IEEE]**,
Department of Mechanical Engineering at Vanderbilt University, Nashville, TN 37235, USA

Dominick S. Ropella* **[Student Member, IEEE]**,
Department of Mechanical Engineering at Vanderbilt University, Nashville, TN 37235, USA

Richard J. Hendrick [Member, IEEE],
Department of Mechanical Engineering at Vanderbilt University, Nashville, TN 37235, USA

Evan Blum,
Department of Mechanical Engineering at Vanderbilt University Medical Center, Nashville, TN 37235, USA.

Robert P. Naftel,
Department of Neurosurgery at Vanderbilt University Medical Center, Nashville, TN 37235, USA.

Hansen C. Bow,
Department of Neurosurgery at Vanderbilt University Medical Center, Nashville, TN 37235, USA.

S. Duke Herrell,
Department of Urologic Surgery at Vanderbilt University Medical Center, Nashville, TN 37235, USA.

Kyle D. Weaver,
Department of Neurosurgery at Vanderbilt University Medical Center, Nashville, TN 37235, USA.

Lola B. Chambless,
Department of Neurosurgery at Vanderbilt University Medical Center, Nashville, TN 37235, USA.

Robert J. Webster III [Senior Member, IEEE]
Department of Mechanical Engineering at Vanderbilt University, Nashville, TN 37235, USA

Abstract

Open surgical approaches are still often employed in neurosurgery, despite the availability of neuroendoscopic approaches that reduce invasiveness. The challenge of maneuvering instruments at the tip of the endoscope makes neuroendoscopy demanding for the physician. The only way to aim tools passed through endoscope ports is to tilt the entire endoscope; but, tilting compresses brain tissue through which the endoscope passes and can damage it. Concentric tube robots can provide necessary dexterity without endoscope tilting, while passing through existing ports in the endoscope and carrying surgical tools in their inner lumen. In this paper we describe the

margaret.rox@vanderbilt.edu.
All authors are members of the Vanderbilt Institute for Surgery and Engineering at Vanderbilt University, Nashville, TN 37235, USA.
*Shared first authorship.

mechatronic design of a new concentric tube robot that can deploy two concentric tube manipulators through a standard neuroendoscope. The robot uses a compact differential drive and features embedded motor control electronics and redundant position sensors for safety. In addition to the mechatronic design of this system, this paper contributes experimental validation in the context of colloid cyst removal, comparing our new robotic system to standard manual endoscopy in a brain phantom. The robotic approach essentially eliminated endoscope tilt during the procedure (17.09° for the manual approach vs. 1.16° for the robotic system). The robotic system also enables a single surgeon to perform the procedure – typically in a manual approach one surgeon aims the endoscope and another operates the tools delivered through its ports.

Keywords

neuroendoscopy; continuum robot; concentric tube robot; robot-assisted surgery; minimally-invasive surgery

I. Introduction

Neurosurgery is in need of advanced robotic instruments. The brain is a sensitive and confined volume, and operating on it requires high accuracy and small, dexterous tools [1]. Based on this, robotics has been applied in neurosurgery since the late 1980s [2]-[4], with much of this early work focused on a stereotactic approach and integration of preoperative imaging. Collaborative neurosurgical robots have also been developed, where the surgeon and the robot hold the tool together, and the surgical field is visualized under a surgical microscope [5]-[7]. The purpose of these systems is to provide better accuracy, steadier hands, or image-guidance while operating in an open surgical setting. For a review of early work on both stereotactic and collaborative systems, see [8].

In parallel with these advancements in robotics, pioneering surgeons have introduced manual rigid endoscopy as a way to reduce invasiveness in comparison to open surgery [9], [10]. Rigid neuroendoscopy offers significant morbidity benefits by eliminating the need for large craniotomies and reducing the volume of healthy brain tissue that must be disrupted to access the surgical site. This reduces the rates of complications including intracerebral hematomas, aphasia, hemiparesis, numbness [11], as well as ventricular collapse and sagging of the brain due to blood and cerebrospinal fluid (CSF) loss [12]. Robotic systems have even been applied to assist with endoscope holding and aiming, with one noteworthy early system being the Aesop of Computer Motion, Inc., which moved in response to physician voice commands [13]. The same basic concept has also been applied to neuroendoscopy (see e.g. [14]). However, endoscope holding robots do not change the fundamental paradigm of tilting the endoscope to both visualize the workspace and manipulate brain tissue [15].

While there are compelling morbidity advantages to an endoscopic approach, wider adoption of endoscopic techniques is limited by how challenging they are to perform safely. Tilting the rigid endoscope (which is the only way to aim surgical tools) is limited to small angles and potentially dangerous [16], since pressure is applied to delicate brain tissue. Surgeons also cite challenges associated with having only a single surgical instrument (in contrast to

two independent instruments in open surgery under a microscope) [10]. With having only one tool deployed through the endoscope, the surgeons lose the ability to provide tension and retraction to the tissue. Shim et al. noted that the field of neuroendoscopy could greatly benefit from innovations in surgical instruments and robotic systems [17]. Greenlee et al. reported in a broad study on endoscopic resection of colloid cysts that "… there is a clear need for improved endoscopic instrumentation to allow precise, bimanual dissection" [18]. The system we describe in this paper is designed to address these needs by delivering two concentric tube robots (see Fig. 1) through the ports in a standard clinical neuroendoscope (Fig. 2), enabling bimanual manipulation and removing the need to tilt the endoscope.

An early robotic system aimed at similar goals was the NeuRobot, which delivered three jointed serial robotic arms through a 10mm diameter custom endoscope [19]. This work is noteworthy in that it was taken all the way through to human clinical trials in Japan [19]. In contrast to the custom system of NeuRobot, the use of concentric tube manipulators in our work enables us to deliver our manipulators through the existing ports in a standard 8.3mm diameter neuroendoscope. Concentric tube manipulators are also straightforward to manufacture in a variety of shapes and sizes [20], providing many new parameters for optimization of robot capabilities based on surgical objectives such as desired workspace and dexterity (see e.g. [21] for an example of optimization for transnasal pituitary surgery). These new parameters arise because concentric tube robots are needle-sized flexible robots composed of superelastic, precurved, concentric tubes that are typically made out of nitinol. The tubes are precurved to a set curvature by heating up the tubes using a method described by [20]. Once the tube is curved, it will retain its shape in free space but will take on the shape of whatever tube it is placed inside (for example, the tube will straighten when placed inside of a straight tube). As the component elastic tubes are translated and rotated with respect to one another, a coordinated, controlled tentacle-like motion can be achieved using mechanics-based models [22], [23] and real-time control methods [22], [24], [25]. For a review of concentric tube robot research, see [26].

Concentric tube robots have been previously suggested for use through flexible endoscopes in neuroendoscopic procedures [27], but new research on torsional windup and snapping in concentric tube robots [28], [29] shows that any overlap of a curved nitinol tube with either a curved endoscope tip or another curved nitinol tube will severely reduce the workspace of the device. Thus, concentric tube robots are better suited to rigid endoscopes where the nitinol transmission can be minimized [30], [31]. Hendrick et al. described a hand-held system that delivered concentric tube manipulators through a rigid endoscope and applied it in the context of prostate surgery [32]. Our system differs from this concept by implementing on-board electronics, a compact drive system, and teleoperation, as our robot is meant to be fixed in place during a procedure. Drake et al. suggested applying this concept in neuroendoscopy in the context of endoscopic third ventriculostomy [33].

Much of the prior work on concentric tube robots, both in the context of endoscopy and in other applications, has focused on feasibility, modeling, and control of the manipulators, with the development of actuation units with embedded motor control left to future work (see e.g. [22], [33]). At the same time, there have been some noteworthy advancements in the design of actuation systems and compact gear transmissions, including the work of

Webster et al. which introduced the differential drive [34], Walsh et al. who introduced the concept a telescoping lead screw combined with a differential drive (as well as a low-cost disposable concept) [35], and the work of Morimoto et al. which used the concept of telescoping screws, while also generalizing the screw to contain gear teeth providing more options for actuator placement [36]. Some of these mechanical concepts, particularly that of Walsh et al. inspired aspects of the system described in this paper. However, our robot differs in that it does not utilize the telescoping concept mentioned in [35], [36], and we package two of the differential drive transmissions into a single system.

A. Contributions

In this paper we contribute the mechatronic design of a new actuation system for actuating two concentric tube robots through the ports of a standard, clinically used endoscope. The actuation system incorporates compact differential drives and redundant sensing. Furthermore, it is modular; each tube is actuated by a copy of the same mechanism. It is the first such system described in the literature with an onboard microcontroller and power electronics for driving the motors. We also contribute the first experiments demonstrating the feasibility of colloid cyst removal with a concentric tube system delivered through an endoscope. We demonstrate for the first time that a robotic system can essentially eliminate endoscope tilting while effectively performing the same procedure.

II. System Design Considerations and Overview

The size, speed, and safety specifications of this neurosurgical robot were determined by considering clinical workflow, safety requirements for current surgical robot systems, and ability to complete desired tasks. Design considerations for our system include:

1. *Size and Weight:* In order to easily integrate into an operating room setting, it is desirable for the robot to be small and light enough to be lifted and moved with one hand.
2. *Tool Velocity:* Previous experiments in neurosurgery determined peak tool velocity to be 1.8 cm/sec when being teleoperated by surgeons [37]. We chose to design for an allowable maximum velocity of 2.5 cm/sec, a target that is a little faster than the peak measured velocity in surgery. The maximum rotational velocity of the tool was designed to be 360 deg/sec. With a known dexterity of the robot, reasonable input velocities from the user should create achievable motor velocities based on motor selection.
3. *Reachable Workspace:* It is desirable to have the workspace of the robot match the endoscope field of view during an operation. The endoscope camera has a depth of view of 20 mm. The camera lens is deployed 5 mm forward from the endoscope tip, meaning the tubes will emerge from the tip before they come into the field of view. The maximum travel of the concentric tube manipulator beyond the tip of the endoscope was determined to be 30 mm to best match the workspace to the field of view.

4. *Redundant Sensing:* Redundant sensing is necessary for safety in surgical robotics [5], [38]; every actuator should have at least two sensors capable of measuring its movement.

5. *Homing:* Automatic homing of the robotic system is necessary for calibration of linear position and rotation for each tube.

6. *Functionality:* The robotic system needs to be capable of performing the same tasks as the manual surgery, and should only require one surgeon to complete the operation. Having two robot arms enables better tissue manipulation through bimanual operation, as the surgeon is able to apply tension and retraction combined with cutting that would not be possible with two manual arms.

Our system, shown in Fig. 2, is composed of a robot, neuroendoscope, and concentric tube manipulators. The tubes extend from the end of a trocar where the surgeon can view the manipulator movement through the endoscope. A surgeon interface and the robot both connect and communicate to a control box via USB. The control box contains a computer to communicate with the devices as well as a DC power supply (Delta, PMT-12V100W1AA) to provide power for the entire system.

A. Tube Modules

The robot body is split into functional units referred to as tube modules, shown in Fig. 3. Since each tube is independently translated and rotated, each module provides two degrees of freedom, and the actuation space of the robot is 8 degrees of freedom. The task space of each arm of the robot was position control in 3 degrees of freedom. Each tube module is electromechanically equivalent and is capable of (1) controlling two DC motors to rotate and translate the tube within it, (2) reading five electronic sensors, and (3) communicating with the control computer. The only connections from the robot to the control box are a power cable and a USB cable, which reduces wiring complexity and weight coming from the robot itself, in comparison to prior robotic systems with off-board motor drivers. Because there is latency/buffering in the USB protocol, the tube modules are daisy-chained, meaning that they are connected serially to one another. Daisy chaining the communication wires also reduced the number of required electrical connections between the tube modules and master control device, simplifying assembly and reducing the likelihood of a bad connection. The I^2C data signal originating from the control box proceeds through all four modules sequentially before returning to the control box. The daisy-chained setup enabled the communication protocol to achieve a fixed communication rate of 250 Hz from the control box to the robot.

B. Differential Drive

Each tube module features a differential drive mechanism, which tends to be more compact than options involving long lead screws, rails, and carriages, or other similar mechanisms, as have been used in many prior prototypes, by both our group and others (see e.g. [22], [24], [27], [30], [32]). A collet nut is used to fix the tube inside the lead screw. The custom stainless steel lead screw features a keyway along the tube axis and mates with two stainless steel spur gears (SDP/SI) (Fig. 4). One spur gear with internal threads translates the lead

screw when driven by a motor, while the other spur gear has a mating key to create a helical, coupled translation/rotation of the lead screw when driven by a motor. A pure rotation can be generated by commanding a differential rotation of both the threaded gear and keyed gear simultaneously. The lead screw length was selected to accommodate the necessary maximum extension of both manipulator arms for the procedure. Both gears are driven by 6 V brushed DC motors (Maxon, DCX10L) with an internal planetary gearhead (Maxon, GPX10) having a gear ratio of 64:1. Motors and lead screw pitch were selected to satisfy instrument velocity design considerations for a maximum tool velocity of 2.5 cm/s, and to be able to overcome internal forces (i.e., friction) to the system. Additional information on the selection process can be found in [39]. The internal structure of the robot is formed by assembling the four modules together. Two modules are assembled along the axis of the endoscope to form the actuation for one arm, and this is mirrored about the midline of the system to create the actuation for the other arm, as demonstrated in Fig. 3. Each lead screw is rigidly fixed to one concentric tube, and each manipulator is fixed to the end of a tube. The inner tube from each manipulator arm pass all the way through the system, so that the surgeon has access to the back ends of the tubes via the back of the robot and can insert tools through their working channels such as suction, cautery, grippers, laser fibers, etc.

C. Concentric Tube Parameters and Model

The parameters of the concentric tubes are as listed in Table I. These parameters provide good overlap between the manipulator workspaces and the endoscope field of view, as shown in Fig. 3. They are an example of a tube set that worked to facilitate our experiments, but we make no claims to optimality. Many results exist for tube optimization (see e.g. [39], [24], [40]), which could be applied to our system in future work.

The mechanics-based model of concentric tubes is well established in the literature [22], [23] and we use it directly. The manipulators are commanded to move in surgeon-specified directions using resolved rates [24]. The surgeon teleoperates each of these arms with visual, endoscopic feedback.

D. Sensors for Redundant Encoding and Homing

The five sensors within the tube module are: two encoders, a digital hall-effect sensor, a magnetic linear position sensor, and a magnetic rotary position sensor. These sensors (except for the encoders) can be seen in Fig. 5. Redundant sensing is important for safety considerations in surgical robotics [38] and the magnetic linear position sensor and the magnetic rotary position sensor were used to add redundancy. The motor position controllers are designed to operate on encoder feedback, but a watchdog timer is used to ensure the redundant sensors match each other for recognition of single fault condition and safety. Matched sensor values reset the watchdog timer, while mismatched readings will fail to reset the timer and eventually trigger a system fault.

The magnetic linear position sensor reads from a linear multi-pole strip magnet that translates with the lead screw. This provides redundant position sensing for the lead screw position in addition to the optical motor encoders, because the motor encoder counts can be converted to linear translation with knowledge of the gear ratios and lead screw pitch. The

magnetic linear position sensor can also sense the end of the magnet, enabling it to be used for translational homing of the lead screw by simply driving the lead screw until the end of the magnet is detected. This design also enables sensing of the backlash present between the motor and the translation of the lead screw which can increase positional accuracy. The magnetic rotary position sensor senses the angular position of the lead screw. This provides redundancy to the motor encoder counts which can be converted to lead screw rotations via the same gear ratios and lead screw pitch as the linear translation redundancy. While this sensor cannot identify an absolute angular position, it can be used for redundant sensing of tube rotation and for backlash detection in the rotation of the tube. To home the angular position of the lead screw we use a digital hall-effect sensor to sense the magnetic field of a small magnet embedded in the hub of the gear that rotates the lead screw. Together, the linear position sensor and digital hall sensor provide automatic homing capabilities for the robot. Rotation and linear position can be homed independently for each tube and the entire robotic system can be homed rapidly, without requiring user input or calibration. The optical encoders on the motors (Maxon, ENX10) were used primarily over the magnetic encoders for control feedback due to better resolution. Optical motor encoders were chosen over absolute motor encoders because they are simpler to interface with and came packaged with the motors.

E. Embedded Motor Control Boards

A block diagram of the tube module control board is shown in Fig. 6. The main component of the control board is the microcontroller (dsPIC33F, Microchip). This microcontroller is designed specifically for motor control applications and includes an interface for standard quadrature encoders. The control board implements a lead-lag controller which updates on a 1 kHz timer interrupt to control the angular position of the motor shaft. The control signal is the duty cycle of a 40 kHz pulse width modulated (PWM) signal, and the loop is closed with incremental optical encoders which are mounted directly to the motors. The PWM signals input to a dual full bridge output motor driver (Avago A4990), which sources power necessary to drive both motors. The magnetic position sensors communicate with the microcontroller via a serial I^2C protocol, and the digital signal from the hall sensor is routed to a digital input pin on the microcontroller.

A separate board with switching regulators takes in 12 V from a power supply in the control box and converts to 3.3 V, 5 V, and 6 V DC power lines for the microcontroller, encoders and sensors, and motors, respectively. A USB to serial converter converts the USB signal to a serial peripheral interface (SPI) protocol.

III. Experiments

We now consider the specific surgical scenario of removing a colloid cyst with the new robotic system described in this paper. Colloid cysts are benign tumors located between the two brain hemispheres in the third ventricle. They account for 2% of primary brain tumors and 15-20% of intraventricular masses [41]-[43] and are one of the types of brain tumors that have been approached endoscopically [18], [44]. As such, colloid cyst removal is a representative application well suited to measuring the endoscopic tilt required to complete a

neurendoscopy procedure. We will then compare the manual approach to a bimanual, robotic approach using our system. To simulate this environment, we created a phantom model inspired by previous work for training surgeons in third ventriculostomy [45]. For our set of experiments, we chose to simulate the colloid cyst resection surgical environment in a phantom based on a patient CT scan.

A. Phantom Design

The colloid cyst from the CT scan sits within the foramen of Monro, as shown in Fig. 7. The cyst is roughly 2 cm in diameter and is approximately spherical. The foramen of Monro, the skull, the cyst, and the ventricles were identified by the participating surgeon (co-author Naftel) as important structures to include in the design of the phantom. Each of these structures was manually segmented from imaging data (Fig. 7).

The ventricles are hollow, open structures full of cerebrospinal fluid, and the foramen of Monro is formed by a circular ring of tissue and is the connecting channel between the lateral and third ventricle. In this CT scan, the cyst is sitting directly within the foramen of Monro. Colloid cysts have a very thin outer membrane and some contain fluid-like contents that can be aspirated. In this phantom design, the colloid cyst is designed to be aspirated. Colloid cysts are also known to have a fibrous “stalk” attachment. This is a thin, string-like structure that attaches the colloid to the superior (i.e. towards the top of the head) surrounding brain anatomy. The cyst is sometimes described as hanging from its stalk within the foramen of Monro.

A silicone molding technique was used to construct the brain phantom. The brain tissue silicone mixture was poured until it completely filled the mold (Fig. 8, left), and left to cure for two hours. The silicone formed around 3D prints of the segmented brain ventricles (Protolabs, PA 850, Black Nylon-11 Selective Laser Sintering), which were removed when the mold was completely cured to leave an empty space for the ventricles. After removing the 3D printed ventricle structure, a pre-molded, stiffer foramen/cyst cavity structure remained in the mold.

The design of the colloid cyst was inspired by the model outlined in [46]. Stretched Parafilm (Heathrow Scientific) was used to form the outer membrane of the cyst, and the cyst was filled with a viscous agarose mixture (Fig. 8, right). The desire was to simulate a colloid cyst where the contents of the cyst could be aspirated, without the contents spilling out of the membrane as soon as it was perforated. As the contents (agarose mixture) are inserted into the cyst, the top of the cyst is tied off with a piece of string to retain the cyst contents. This piece of string simulates the fibrous “stalk” that attaches the colloid cyst to its surrounding brain anatomy. The cyst is then manually placed into ventricles, so that it hangs from its superiorly-attached simulated stalk, as can be seen in Fig. 9 from the outside (left) and through the endoscope view (right).

B. Experimental Procedure

To begin the experiments, an entry burr hole was drilled by the experimenting neurosurgeon into the skull phantom. The trajectory was planned by eye, and the surgeon drilled the burr hole to a diameter just larger than the endoscope. The endoscope/trocar used in this

experiment is the Minop Invent 30° neuroendoscope (Aesculap, Inc.). The manual procedure was completed with two surgeons: an experienced pediatric neurosurgeon and a neurosurgical fellow. The neurosurgical fellow was in control of the hand tools that pass through the working channel of the trocar, and the pediatric neurosurgeon was in control of the endoscope/trocar. For the robotic procedure, the neurosurgeon is in sole control and teleoperates both arms, and the endoscope is secured by a holding arm. The position of the manipulators is controlled by the surgeon interface, for this case: two haptic user input devices (Novint Falcon, Novint Technologies, Inc.), one for each manipulator. The user interfaces were programmed in C++ to interact with the robot.

There are three basic stages to the experiment; first, the surgeon must perforate the thin cyst membrane with a gripper so that the gelatinous contents begin to spill out. Second, the surgeon aspirates the cyst contents until the cyst is sufficiently debulked. Lastly, the surgeon must find the stalk attachment point (i.e. the string) and place the tool on the string to simulate the cut that is required to free the cyst and remove it. In the experiment, as soon as the tool is placed on the string, the experiment is considered complete, and the surgeon is not required to actually cut the string. During the manual experiment, two tools are used sequentially: forceps and an aspiration tube. First, the forceps are inserted into the tool channel and used to perforate the cyst. The surgeon then removes the forceps in exchange for a flexible aspiration tube which is connected to vacuum, and then switches back to the forceps to simulate cutting the stalk. The tools can be changed as desired during the procedure, but it takes time to switch from one to the other. For the robotic experiment, the surgeon has the ability to aspirate with the left arm throughout the entire procedure and has forceps in the right manipulator for the entire procedure. Since the forceps opening and closing degree of freedom had not been motorized at the time of the experiment, the forceps were actuated manually by the assisting engineer when the surgeon verbally requested that they be opened or closed.

We tracked the movement of the endoscope during both the manual and the robotic experiment using NDI Optotrak (Northern Digital, Inc.) in six degrees of freedom. The Optotrak was rigidly mounted to a wall and the experimental setup was within the workspace of the tracking system. A frame with optical tracking markers was mounted to the endoscope to measure the movements of the endoscope during both the manual and the robotic experiments. For the manual experiment, we also tracked the 1D insertion-retraction motion of the forceps, and the tip location during the procedure could be measured through the geometric relationship of the tracking markers to the tool tips. During the robotic procedure, the motions of the tool tips were recorded using the kinematics of the concentric tube manipulators.

The experiment begins with the endoscope in a neutral (i.e. not tilted) configuration with the forceps at the tip of the endoscope. This enables tracking of the tip of the forceps relative to the endoscope tip and the tilt of the endoscope relative to its neutral configuration at the beginning of the procedure. The endoscope angle ε is calculated by tracking the z axis of the endoscope, which is the axis that runs along the length of the endoscope. The change in angle is measured from the neutral configuration, i.e. the position of the endoscope in its starting configuration.

For the robotic experiment, the robotic system/endoscope is held by a passive, lockable arm and the surgeon teleoperates the concentric tube manipulators with the haptic user input devices. The user interface maintains the surgeon's hands within the boundaries of the endoscope view by providing virtual walls, which apply forces to the surgeon's hands if he/she attempts to move outside the endoscope field of view. A push-button is provided on the interface that can be used for clutching. The scaling between the surgeon's hand motion and the manipulator motion can be changed on demand during teleoperation by the surgeon. The passive arm was allowed to be reconfigured if needed by the surgeon during the procedure, and any reconfiguration of the system would be optically tracked and recorded. The experiment was started in both the manual and robotic cases when the surgeon was satisfied with the position of the endoscope/tools. In both cases, the surgeon verified the tools could reach the cyst prior to initiating the recording of the experimental data through the use of a 3D visual display and by calculating the distance between the tip of the endoscope and the object to ensure that the robot would reach.

C. Results

The endoscopic angulation ε for both the manual and robotic experiments are shown in Fig. 10 and summarized in Table II.

The mean endoscope angulations were 3.97° and 0.46° for the manual and robotic experiments, respectively. The max endoscope angulations were 17.09° and 1.16° for the manual and robotic experiments, respectively. The surgeon was able to accomplish the entire robotic procedure without reconfiguring the endoscope.

The movement of the endoscope in this case is the result of bumps, vibrations, tracking noise, and flexibility of the robot/endoscope structure. Note that tracking was temporarily lost due to line-of-sight obstructions for 0.42 s during the manual procedure and 14.35 s during the robotic experiment. The calculations for ε in Table II do not include times when tracking was lost, but the experiment time does.

In Fig. 10 (Top), the stages were defined to begin/end when the tool was exchanged, and in Fig. 10 (Bottom), the stages were approximated to begin/end based on the visual motions in the endoscopic video feed. The most noteworthy results from Fig. 10 are that (1) it was possible to complete the robotic procedure without reconfiguring the endoscope, (2) endoscopic angulation as high as 17.09° was observed during the manual procedure in the stalk cut stage of the procedure, and (3) 5-10° oscillations in endoscopic angulation were common during the manual procedure. The maximum extension of the tool from the endoscope tip was found to be 23.1 mm.

The locations, relative to the registered anatomy, that the tips of the tools reached for both the manual and robotic procedure are shown in Fig. 11(a)-(c). Recall that the aspiration tube movements during the manual procedure were not tracked due to the flexibility of the tube. For the manual procedure, the locations of the tool tip during the cyst perforation stage and the cyst cut stage of the procedure are clearly grouped (shown within ellipses in Fig. 11(a)). The point clouds are highly axial, as one would expect since these points are generated by axial extension/retraction of the tool through the endoscope. As is shown in Fig. 10 (Top),

the endoscope moves considerably, approximately 10-15° between these two stages of the procedure. The corresponding robotic manipulator positions for the cyst perforate/cut stages of the procedure are shown in Fig. 11(b)). As is clear from this Figure, the manipulator tips each move considerably less than the forceps did during the manual procedure. It is also clear that both manipulator arms are used together during the perforation/cut portions of the procedure. Fig. 11(a)-(c) also shows the manipulator tip positions during the entire experiment; the point clouds approximate the conical workspace that the manipulator tips were constrained to operate within. It appears that during the robotic procedure, the manipulators did not reach the same locations that were accessed during the manual cut portion of the experiment. This is because the endoscope did not move; instead, the surgeon used the bimanual capability of the manipulators to orient the cyst with the right arm so that the string was exposed and then touched the string with the left arm. The positions that the endoscope tip reached during both the manual and robotic experiment are shown in Fig. 11(d)-(e).

It is possible to quantify the total motion of the tool tips that was required during the manual and robotic experiments. This data is summarized in Table III. The tracking data for the manual procedure and the logged tip position data for the robotic procedure were both down-sampled to 10 Hz for this analysis. This was done to reduce the impact of the high frequency tracking noise when calculating the distance between subsequent tip positions. The tip distance traveled by the forceps during the perforation stage of the manual procedure was 479 mm. In comparison, the tip distance traveled by the left and right manipulator was 201 mm and 218 mm, respectively. The total distance moved was similar between the manual and robotic procedures, but these motions were split over two arms in the robotic portion of the procedure. On average, the manual forceps moved about twice as fast as the robotic manipulators during the experiment. Similar results were found during the cutting stage of the procedure.

IV. DISCUSSION

In addition to the quantitative results in the prior section, it was qualitatively clear that the motions being made manually versus robotically were different, due primarily to the presence of a second arm. Fig. 12 shows an example of these qualitative differences for each of the stages of the procedure.

For example, first consider the cyst perforation stage of the procedure. When done manually, the neurosurgeon aligned the endoscope so that the forceps could extend straight to the membrane of the cyst and grab it. Because the surgeon had no ability to apply retraction, when the forceps grabbed the cyst and pulled on it, the entire cyst was displaced towards the tip of the endoscope rather than perforating the membrane. To actually perforate the membrane, the surgeon twisted/poked the forceps into the membrane until it eventually perforated. In contrast, during the robotic experiment, the surgeon was able to grasp the cyst with the right manipulator (forceps), apply tension, and use the left manipulator to open up the cyst, as is shown in Fig. 12(b).

Similarly, during the manual aspiration stage of the procedure, the aspiration tube was poked into the cyst until it was satisfactorily debulked. Some aiming of the aspiration tube was possible by tilting the endoscope. In contrast, during the robotic experiment, the surgeon was able to hold the cyst with the right manipulator and aspirate from the floor with the left manipulator. The surgeon also opened the cyst with the forceps and inserted the aspiration manipulator inside of the cyst. Another maneuver the surgeon utilized during this stage of the procedure was to press against the cyst with the right manipulator and force out the cyst contents and aspirate simultaneously. Lastly, during the manual procedure, at the stalk cutting stage, a large endoscopic angle was required to reach the stalk, as one can see quantitatively in Fig. 10 (Top), and qualitatively in Fig. 12(e). In contrast, during the robotic experiment, the surgeon used the manipulator forceps to manipulate the cyst (i.e. moving the anatomy to the tools) towards the left manipulator. Once the string was in range of the left arm, it reached out and touched the string; this type of maneuver was not possible with a single, manual tool and endoscopic angulation.

There is another element of this procedure that changed when switching from a manual procedure to a robotic procedure: the number of surgeons required was reduced from two to one, and the number of hands that are located near the base of the endoscope is reduced from four to zero. During the manual procedure, coordinated motions and efficient communication are required to accomplish the surgical task – since one surgeon is in control of the endoscope and the other is in control of the tool. This effectively means one surgeon controls the axis of the endoscopic tool and the visualization, while the other controls the extension, retraction, and actuation of the transendoscopic tool. The robotic setup reduces this complexity, returns this to a single surgeon procedure, and eliminates the coordination/communication requirement.

A. Future Work

We hypothesize that the tool motions required for the robotic system can be reduced even further (in comparison to those presented in Table III). As the user interface is refined and the surgeon gains more experience teleoperating this system, the surgeon would likely require less time and movement to accomplish the tasks. This was the experimenting surgeon’s first interaction with the robotic system system. Further, the motion of the tubes can be distracting to the surgeon in the endoscopic view; as the tubes move relative to one another, it can be difficult for the surgeon to focus on the tip of the manipulator. A sheath that hides the relative tube motions would likely help to address this concern. We anticipate that these refinements will show, even more clearly, the change in surgical approach that is possible when provided with bimanual dexterous manipulators, and we hypothesize that it may eventually be possible for the robotic system to be more efficient than the manual procedure.

Future optimization work can be done to maximize the overlap between the workspace of the concentric tubes and the endoscope field of view, similar to concentric tube optimization for prostate surgery [32]. There is also opportunity to design the system for sterility, which has already been done for concentric tube robots used in intracerebral hemorrhage surgery [47].

V. Conclusion

These phantom experiments showed that this two-arm concentric tube robot system could be used to complete the tasks required for endoscopic surgical treatment of colloid cysts, without necessitating endoscopic angulation. We also found that the arms moved less during each stage of the robotic procedure than they did during the corresponding stage of the manual experiment, and that the manipulator tips generally moved more slowly in the robotic case. Qualitatively, the presence of a second, dexterous tool completely changed the surgical approach. In particular, the ability to apply tension, retraction, and use the arms cooperatively enabled the surgeon to perform more complex surgical maneuvers to manipulate the cyst, without requiring endoscope angulation.

Acknowledgments

This material is based upon work supported by the National Institutes of Health under NIH-NIBIB training grant T32EB021937. Any opinions, findings, and conclusions or recommendations expressed in this material are those of the authors and do not necessarily reflect the views of the NIH or the NIBIB.

Biography

Margaret F. Rox (S’17) received the B.S. degree in mechanical engineering from Lipscomb University, Nashville, TN, USA, in 2016. She is currently working toward the Ph.D. degree in mechanical engineering at Vanderbilt University, Nashville, TN, USA.

She is involved in the research of medical robotics, continuum robotics, and endoscopic robot design and control. She is currently with the Medical Engineering and Discovery Laboratory.

Dominick S. Ropella (S’19) received the B.S. degree in mechanical engineering from Marquette University in Milwaukee, WI, USA, in 2018. Since then, he has been working toward the Ph.D. degree in mechanical engineering at Vanderbilt University, Nashville, TN, USA.

He is involved in the research of medical robotics and continuum robotics. He is currently with the Medical Engineering and Discovery Laboratory.

Richard J. Hendrick (S'12-M'17) received the B.S. degree in biomedical engineering from Texas A&M University, College Station, TX, USA, in 2011, and the M.S. and Ph.D. degrees in mechanical engineering at Vanderbilt University, Nashville, TN, USA, in 2017.

He is currently the Chief Operating Officer of Virtuoso Surgical, Inc.

Evan Blum received the B.S. degree in mechanical engineering from Vanderbilt University, Nashville, TN, USA in 2017. He worked as an undergraduate in the Medical Engineering and Discovery Laboratory.

He is currently a robotics engineer at Virtuoso Surgical, Inc.

Robert P. Naftel received the B.A. degree in chemistry from Washington and Lee University, Lexington, VA, USA and the M.D. degree from the University of Alabama at Birmingham, AL, USA. He completed his residency in Neurosurgery at the University of Alabama, as well as a fellowship in Pediatric Neurosurgery at the University of Pittsburgh, Pittsburgh, PA, USA.

He is currently an associate professor of neurological surgery and the pediatric neurosurgery fellowship director at the Vanderbilt University Medical Center, Nashville, TN, USA. While in residency, he received the Resident Leadership Award and the James A. Nobles Neurosurgery Book Award. In 2011, the Congress of Neurological Surgeons honored him with the Sherry Apple Resident Travel Scholarship for his research on the role of neuroendoscopy in the treatment of hydrocephalus.

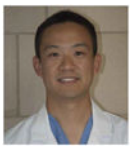

Hansen C. Bow received the B.S. degree in electrical engineering and computer science from the University of California, Berkeley, CA, USA, and the M.S. and Ph.D. degrees in electrical engineering and computer science from the Massachusetts Institute of Technology,

Cambridge, MA, USA. He received the M.D. degree from Johns Hopkins University School of Medicine, Baltimore, MD, USA.

He is currently in residency in the Department of Neurological Surgery at Vanderbilt University Medical Center, Nashville, TN, USA.

S. Duke Herrell received the B.A. degree in chemistry from the University of Richmond, Richmond, VA, USA, and the M.D. degree from the University of Virginia School of Medicine, Charlottesville, VA, USA.

He is a professor of urologic surgery at Vanderbilt University School of Medicine, Nashville, TN, USA, and a professor of biomedical engineering and mechanical engineering within Vanderbilt's School of Engineering. He also serves as Director of Robotic Surgery for the Vanderbilt Medical Center. He established the Robotics and minimally-invasive urologic surgery programs at Vanderbilt and has an active clinical practice in robotic renal and prostate surgery, utilizing advanced endoscopic and ablative technologies. He holds several patents for medical devices and co-founded Virtuoso Surgical, Inc.

Kyle D. Weaver received the B.S. degree in psychology from Duke University, Durham, NC, USA, and received the M.D. degree from and completed his neurosurgical training at the University of North Carolina at Chapel Hill, NC, USA. He then completed a brain tumor fellowship at The Johns Hopkins University, Baltimore, MD, USA.

He joined the faculty of the Department of Neurological Surgery, Vanderbilt University Medical Center, Nashville, TN, USA, in 2004, where he co-directed the Vanderbilt Pituitary Center while holding a joint appointment in otolaryngology and taking an active role in the Vanderbilt Brain Tumor and Skull Base Programs.

Lola B. Chambless received the B.S. degree in biological sciences from Stanford University, Stanford, CA, USA, and the M.D. degree from the Vanderbilt University School of Medicine, Nashville, TN, USA. She completed her residency in Neurological Surgery and fellowship in Neurosurgical Oncology at Vanderbilt. She also completed a fellowship in

Minimally Invasive Neurosurgical Oncology at the Centre for Minimally Invasive Neurosurgery in Sydney, Australia.

She is currently an associate professor of neurological surgery and radiation oncology at Vanderbilt University Medical Center. She is also the Residency Program Director in Neurological Surgery at Vanderbilt and is currently serving as a Member-at-Large for the Congress of Neurological Surgeons (CNS) co-chairing the CNS Leadership Institute.

Robert J. Webster, III (S'97-M'08-SM'14) received the B.S. degree in Electrical Engineering from Clemson University, Clemson, SC, USA, in 2002, and the M.S. and Ph.D. degrees in Mechanical Engineering from the Johns Hopkins University, Baltimore, MD, USA, in 2004 and 2007, respectively.

Since 2008 he has been a faculty member at Vanderbilt University, Nashville, TN, USA, where he currently holds the Richard A. Schroeder Chair in Mechanical Engineering and is a Professor of Mechanical Engineering, Electrical Engineering, Otolaryngology, Neurological Surgery, Urologic Surgery, and Medicine (Interventional Pulmonology). He directs the Medical Engineering and Discovery Laboratory and is a co-founder and a steering committee member for the Vanderbilt Institute for Surgery and Engineering, which brings together physicians and engineers to solve challenging clinical problems. He serves as a Charter Member of the NIH Imaging Guided Interventions and Surgery study section. He is Founder President of Virtuoso Surgical, Inc., and EndoTheia, Inc., Nashville, TN, USA. His research interests include surgical robotics, image-guided surgery, and continuum robotics.

Dr. Webster is a recipient of the IEEE Robotics and Automation Society Early Career Award, the National Science Foundation CAREER Award, the Robotics Science and Systems Early Career Spotlight Award, the IEEE Volz Award, and the Vanderbilt Engineering Award for Excellence in Teaching. He has served as Chair of the International Society for Optics and Photonics Image-Guided Procedures, Robotic Interventions, and Modeling Conference, Associate Editor of IEEE Transactions on Robotics, and currently serves as Associate Editor for the International Journal of Robotics Research.

References

[1]. Wang MY, Goto T, Tessitore E, and Veeravagu A, "Introduction. Robotics in neurosurgery," Neurosurgical Focus, vol. 42, no. 5, p. E1, 5 2017.

[2]. Benabid A, Cinquin P, Lavalle S, Le Bas J, Demongeot J, and de Rougemont J, "Computer-driven robot for stereotactic surgery connected to CT scan and magnetic resonance imaging," Stereotactic and Functional Neurosurgery, vol. 50, no. 1-6, pp. 153–154, 1987.

[3]. Kwoh Y, Hou J, Jonckheere E, and Hayati S, "A robot with improved absolute positioning accuracy for CT guided stereotactic brain surgery," IEEE Transactions on Biomedical Engineering, vol. 35, no. 2, pp. 153–160, 1988. [PubMed: 3280462]

[4]. Davies B, “A review of robotics in surgery,” Proceedings of the Institution of Mechanical Engineers Part H Journal of Engineering in Medicine, vol. 214, no. 1, pp. 129–140, 1 2000.

[5]. Nathoo N, Çavuşoğlu MC, Vogelbaum MA, and Barnett GH, “In touch with robotics: Neurosurgery for the future,” Neurosurgery, vol. 56, no. 3, pp. 421–433, 3 2005. [PubMed: 15730567]

[6]. Taylor RH, Jensen P, Whitcomb L, Barnes A, Kumar R, Stoianovici D, Gupta P, Wang Z, deJuan E, and Kavoussi L, “A steady-hand robotic system for microsurgical augmentation,” Int. J. Robot. Res, vol. 18, no. 12, pp. 1201–1210, 12 1999.

[7]. Rizun PR, McBeth PB, Louw DF, and Sutherland GR, “Robot-assisted neurosurgery,” Seminars in Laparoscopic Surgery, vol. 11, no. 2, pp. 99–106, 2004. [PubMed: 15254648]

[8]. Taylor R and Stoianovici D, “Medical robotics in computer-integrated surgery,” IEEE Trans. Robot. Autom, vol. 19, no. 5, pp. 765–781, 10 2003.

[9]. Sgouros S, Ed., Neuroendoscopy: current status and future trends. New York, NY: Springer Berlin Heidelberg, 2014.

[10]. Zada G, Liu C, and Apuzzo ML, ““Through the looking glass”: Optical physics, issues, and the evolution of neuroendoscopy,” World Neurosurgery, vol. 79, no. 2, pp. S3–S13, 2 2013. [PubMed: 23391453]

[11]. Andrews RJ and Bringas JR, “A Review of Brain Retraction and Recommendations for Minimizing Intraoperative Brain Injury,” Neurosurgery, vol. 33, no. 6, pp. 1052–1064, 12. 1993. [PubMed: 8133991]

[12]. Lee YH, Kwon YS, and Yang KH, “Multiloculated hydrocephalus : Open craniotomy or endoscopy?” Journal of Korean Neurosurgical Society, vol. 60, no. 3, pp. 301–305, 5 2017. [PubMed: 28490156]

[13]. Allaf ME, Jackman SV, Schulam PG, Cadeddu JA, Lee BR, Moore RG, and Kavoussi LR, “Laparoscopic visual field, voice vs foot pedal interfaces for control of the aesop robot,” Surgical Endoscopy, vol. 12, no. 12, pp. 1415–1418, 12 1998. [PubMed: 9822469]

[14]. Zimmermann M, Krishnan R, Raabe A, and Seifert V, “Robot-assisted navigated endoscopic ventriculostomy: implementation of a new technology and first clinical results,” Acta Neurochirurgica, vol. 146, no. 7, 7 2004.

[15]. Hopf NJ and Perneczky A, “Endoscopic Neurosurgery and Endoscope-assisted Microneurosurgery for the Treatment of Intracranial Cysts,” Neurosurgery, vol. 43, no. 6, pp. 1330–1336, 12 1998. [PubMed: 9848846]

[16]. Teo C, Rahman S, Boop FA, and Cherny B, “Complications of endoscopic neurosurgery,” Child’s Nervous System, vol. 12, no. 5, pp. 248–253, 5 1996.

[17]. Shim KW, Park EK, Kim D-S, and Choi J-U, “Neuroendoscopy : Current and future perspectives,” Journal of Korean Neurosurgical Society, vol. 60, no. 3, pp. 322–326, 5 2017. [PubMed: 28490159]

[18]. Greenlee JD, Teo C, Ghahreman A, and Kwok B, “Purely endoscopic resection of colloid cysts,” Operative Neurosurgery, vol. 62, no. suppl_1, pp. ONS51–ONS56, 3 2008.

[19]. Takasuna H, Goto T, Kakizawa Y, Miyahara T, Koyama J, Tanaka Y, Kawai T, and Hongo K, “Use of a micromanipulator system (neurobot) in endoscopic neurosurgery,” Journal of Clinical Neuroscience, vol. 19, no. 11, pp. 1553–1557, 11 2012. [PubMed: 22995760]

[20]. Gilbert HB and Webster RJ, “Rapid, reliable shape setting of superelastic nitinol for prototyping robots,” IEEE Robotics and Automation Letters, vol. 1, no. 1, pp. 98–105, 1 2016. [PubMed: 27648473]

[21]. Burgner J, Gilbert HB, and Webster III RJ, “On the Computational Design of Concentric Tube Robots: Incorporating Volume-Based Objectives,” in IEEE International Conference on Robotics and Automation, 2013, pp. 1185–1190.

[22]. Dupont P, Lock J, Itkowitz B, and Butler E, “Design and control of concentric-tube robots,” IEEE Transactions on Robotics, vol. 26, no. 2, pp. 209–225, 4 2010. [PubMed: 21258648]

[23]. Rucker DC, Jones BA, and Webster III RJ, “A geometrically exact model for externally loaded concentric-tube continuum robots,” IEEE Transactions on Robotics, vol. 26, no. 5, pp. 769–780, 10 2010. [PubMed: 21566688]

[24]. Burgner J, Rucker DC, Gilbert HB, Swaney PJ, Russell PT, Weaver KD and Webster RJ, "A telerobotic system for transnasal surgery," IEEE/ASME Transactions on Mechatronics, vol. 19, no. 3, pp. 996–1006, 6 2014.

[25]. Xu R and Patel RV, "A fast torsionally compliant kinematic model of concentric-tube robots." IEEE, 8 2012, pp. 904–907.

[26]. Mahoney AW, Gilbert HB, and Webster III RJ, A Review of Concentric Tube Robots: Modeling, Control, Design, Planning, and Sensing, 2016, vol. Minimally Invasive Surgical Robotics.

[27]. Butler EJ, Hammond-Oakley R, Chawarski S, Gosline AH, Codd P, Anor T, Madsen JR, Dupont PE, and Lock J, "Robotic neuroemdoscope with concentric tube augmentation." IEEE, 10 2012, pp. 2941–2946.

[28]. Dupont P, Lock J, and Butler E, "Torsional kinematic model for concentric tube robots." IEEE, 5 2009, pp. 3851–3858.

[29]. Hendrick RJ, Gilbert HB, and Webster III RJ, "Designing snap-free concentric tube robots: A local bifurcation approach," in IEEE International Conference on Robotics and Automation, 2015, pp. 2256–2263.

[30]. Lin F-Y, Bergeles C, and Yang G-Z, "Biometry-based concentric tubes robot for vitreoretinal surgery." IEEE, 8 2015, pp. 5280–5284.

[31]. Lathrop R, Bruns TL, Mahoney AW, Gilbert HB, Swaney PJ, Hendrick RJ, Weaver K, Russell PT, Herrell SD, and Webster RJ, "Modular sterilizable robotic system for endonasal surgery," US Patent US10307214B2, 6., 2019.

[32]. Hendrick RJ, Mitchell CR, Herrell SD, and Webster RJ, "Hand-held transendoscopic robotic manipulators: A transurethral laser prostate surgery case study," The International Journal of Robotics Research, vol. 34, no. 13, pp. 1559–1572, 11 2015. [PubMed: 27570361]

[33]. Bodani VP, Azimian H, Looi T, and Drake JM, "104-design and evaluation of a concentric tube robot for minimally-invasive endoscopic pediatric neurosurgery," Neurosurgery, vol. 61, p. 192, 8 2014.

[34]. Webster RJ, Swensen JP, Romano JM, and Cowan NJ, "Closed-Form Differential Kinematics for Concentric-Tube Continuum Robots with Application to Visual Servoing," in Experimental Robotics, ser. Springer Tracts in Advanced Robotics. Springer, 2009, pp. 485–494. https://scholar.google.com/scholar?hl=en&as_sdt=0%2C43&q=Closed-Form+Differential+Kinematics+for+Concentric-Tube+Continuum+Robots+with+Application+to+Visual+Servoing&btnG=

[35]. Torabi M, Gupta R, and Walsh CJ, "Compact robotically steerable image-guided instrument for multi-adjacent-point (map) targeting," IEEE Transactions on Robotics, vol. 30, no. 4, pp. 802–815, 8 2014.

[36]. Morimoto TK, Hawkes EW, and Okamura AM, "Design of a compact actuation and control system for flexible medical robots," IEEE Robotics and Automation Letters, vol. 2, no. 3, pp. 1579–1585, 7 2017. [PubMed: 28664187]

[37]. Swaney PJ, Croom JM, Burgner J, Gilbert HB, Rucker DC, Webster RJ, Weaver KD, and Russell PT, "Design of a Quadramanual Robot for Single-Nostril Skull Base Surgery." American Society of Mechanical Engineers Digital Collection, 9. 2013, pp. 387–393.

[38]. Kazanzides P, Fichtinger G, Hager GD, Okamura AM, Whitcomb LL, and Taylor RH, "Surgical and Interventional Robotics," IEEE robotics & automation magazine, vol. 15, no. 2, pp. 122–130, 6. 2008. [PubMed: 20428333]

[39]. Hendrick R, "System Design and Elastic Stability Modeling of Transendoscopic Continuum Robots," Ph.D. Dissertation, Nashville, TN, 2017.

[40]. Bergeles C, Gosline AH, V Vasilyev N, Codd PJ, del Nido PJ, and Dupont PE, "Concentric tube robot design and optimization based on task and anatomical constraints," IEEE Transactions on Robotics, vol. 31, no. 1, pp. 67–84, 2 2015. [PubMed: 26380575]

[41]. Kornienko VN and Pronin IN, Diagnostic neuroradiology. Am Soc Neuroradiology, 2009.

[42]. Osborn AG and Preece MT, "Intracranial cysts: Radiologic-pathologic correlation and imaging approach," Radiology, vol. 239, no. 3, pp. 650–664, 6 2006. [PubMed: 16714456]

[43]. Waggenspack G and Guinto F, "MR and CT of masses of the antero-superior third ventricle," American Journal of Roentgenology, vol. 152, no. 3, pp. 609–614, 3 1989. [PubMed: 2783815]

[44]. Souweidane MM, “Endoscopic management of pediatric brain tumors,” Neurosurgical Focus, vol. 18, no. 6, pp. 1–6, 6 2005.

[45]. Breimer GE, Bodani V, Looi T, and Drake JM, “Design and evaluation of a new synthetic brain simulator for endoscopic third ventriculostomy,” Journal of Neurosurgery Pediatrics, vol. 15, no. 1, pp. 82–88, 1 2015. [PubMed: 25360853]

[46]. Manjila S, Mencattelli M, Rosa B, Price K, Fagogenis G, and Dupont PE, “A multiport MR-compatible neuroendoscope: spanning the gap between rigid and flexible scopes,” Neurosurgical Focus, vol. 41, no. 3, p. E13, 9. 2016.

[47]. Burgner J, Swaney PJ, Lathrop RA, Weaver KD, and Webster RJ, “Debulking from within: A robotic steerable cannula for intracerebral hemorrhage evacuation,” IEEE Transactions on Biomedical Engineering, vol. 60, no. 9, pp. 2567–2575, 9 2013. [PubMed: 23649131]

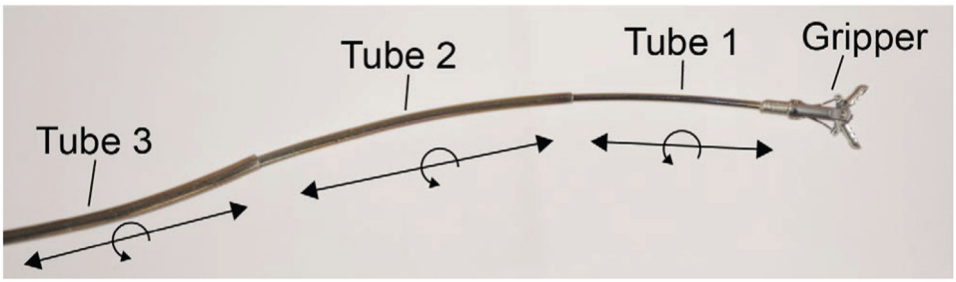

Fig. 1:

A three-tube concentric tube robot consisting of precurved nitinol tubes nested inside of each other. Each tube can translate and rotate, and various tools can be deployed through the inner lumen. Our robotic system utilizes this same concept with two precurved nitinol tubes for each concentric tube robot and two robots deployed side by side through the endoscope.

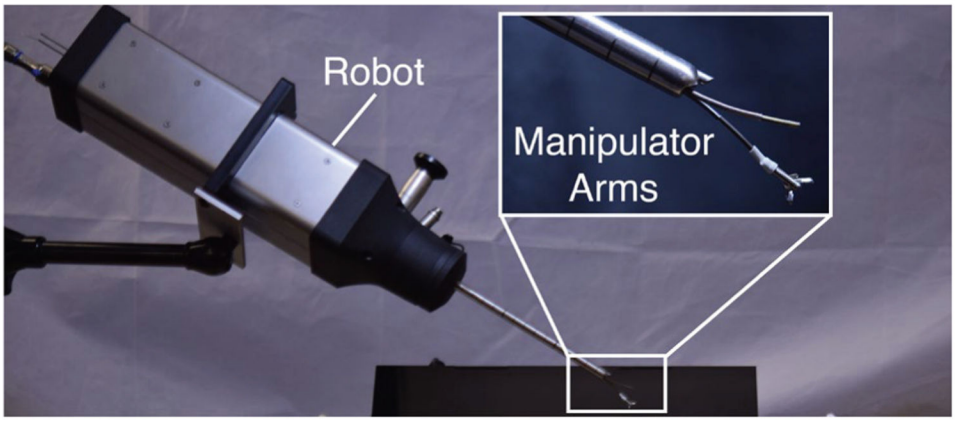

Fig. 2:
Our compact robotic system delivers two concentric tube manipulators through the port in a standard clinical neuroendoscope, providing dexterity at the surgical site.

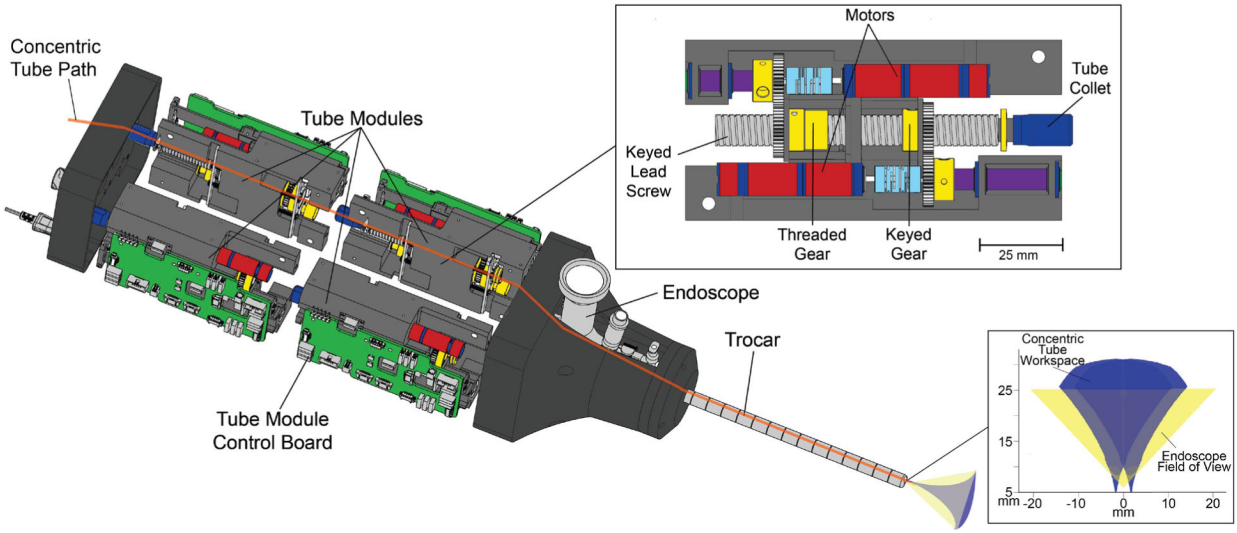

Fig. 3:

Robot without outer housing. There are four tube modules, an example of which is shown in the magnified view. Two identical modules are lined up along the axis of their lead screws, which makes a half. The half is mirrored and held together along the axis of the endoscope/trocar. The back modules control the inner tube translation and rotation, while the front modules control the outer tube. The threaded gear moves the lead screw to translate the tube, while the keyed gear will translate and rotate the tube. Moving the threaded gear and keyed gear simultaneously commands a pure rotation. On the bottom right of this image can be seen the workspace of the concentric tube manipulators as well as the field of view of the endoscope.

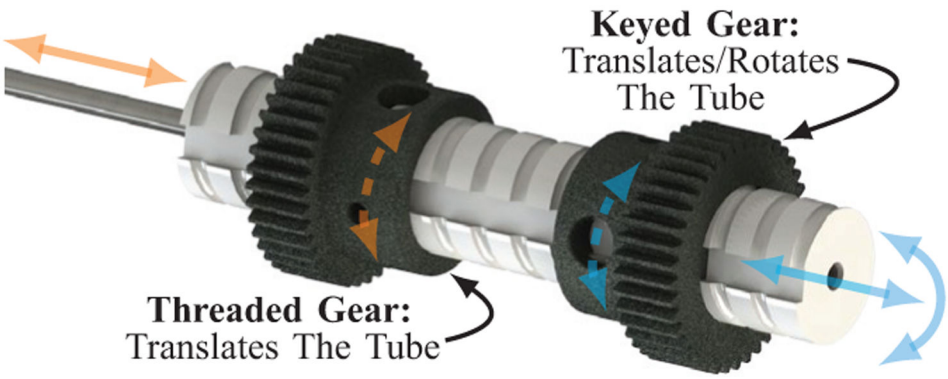

Fig. 4:
A close up of the keyed lead screw mechanism showing the details of its differential drive actuation.

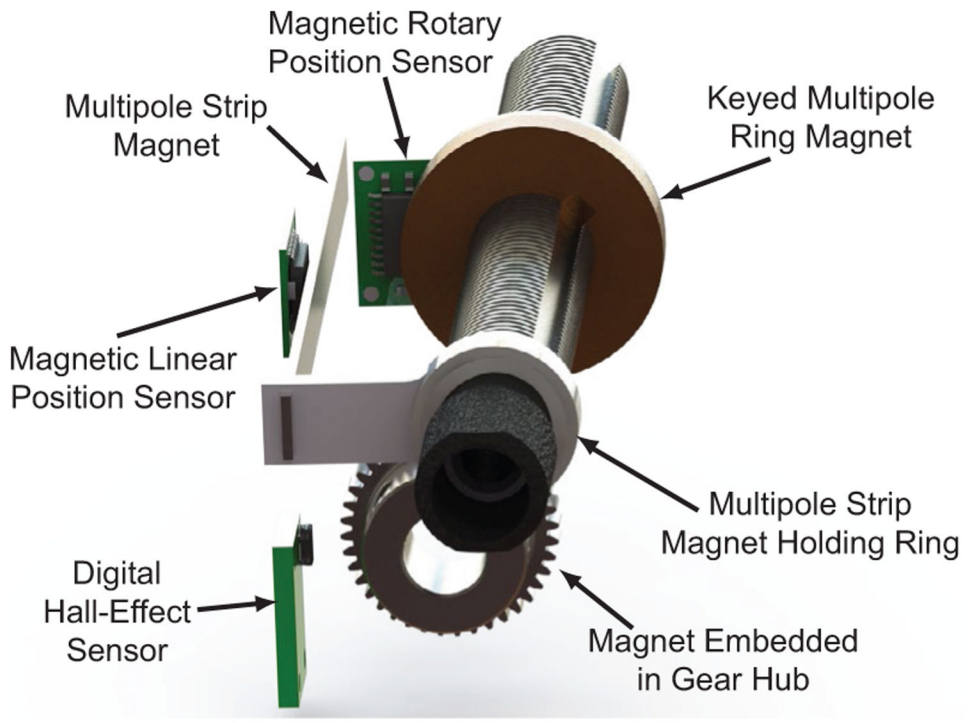

Fig. 5:

The magnetic sensors featured within the tube module. The translation of the tube is sensed with the linear position sensor, the rotation of the tube is sensed with the rotary position sensor and homed with the digital hall-effect sensor.

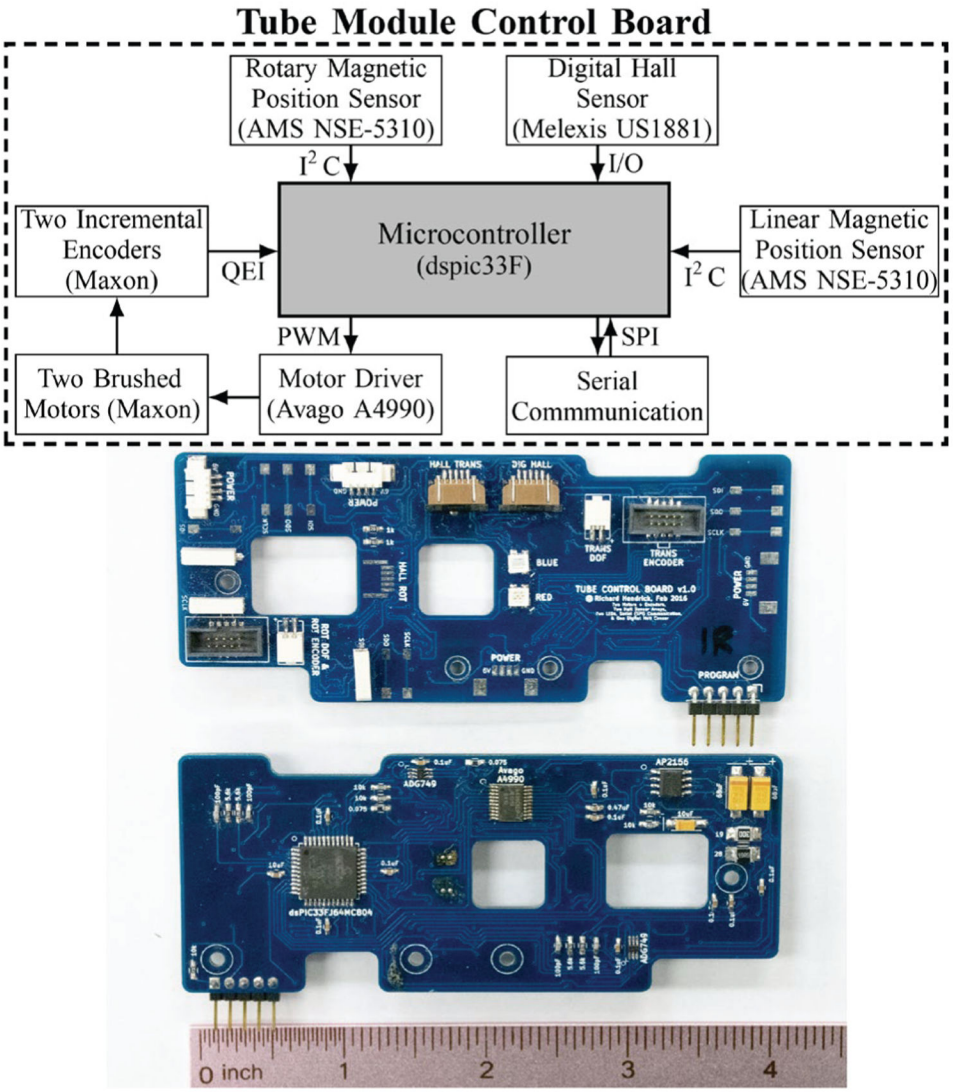

Fig. 6:

Top: Block diagram demonstrating flow of information on the embedded motor control board. Bottom: front and back of embedded motor control board.

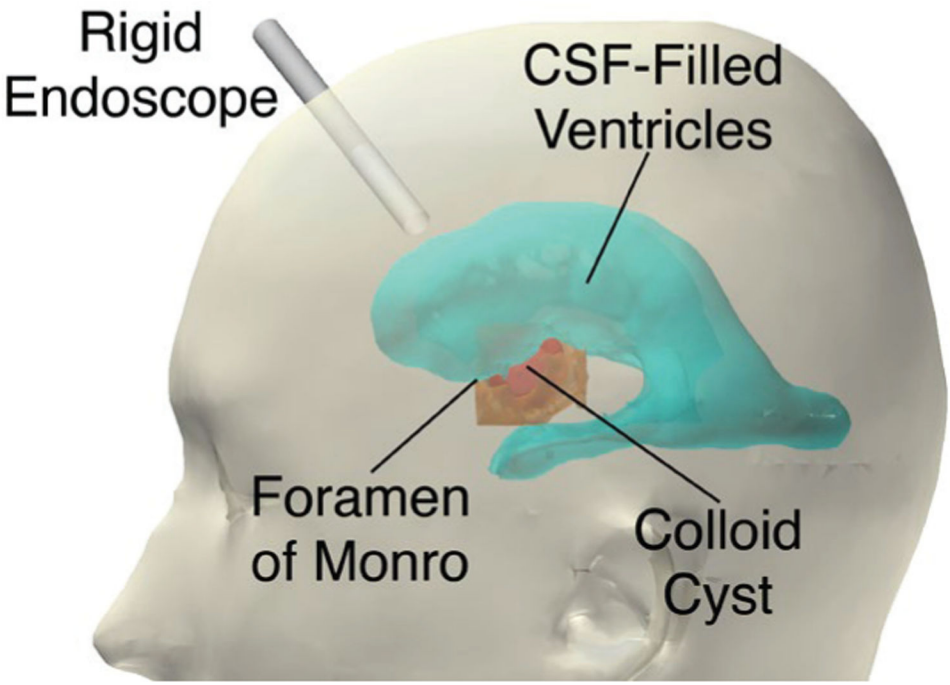

Fig. 7:

Ventricles, colloid cyst, foramen of Monro, and skull were segmented from a CT scan. For endoscopic removal of a colloid cyst, the rigid endoscope is inserted through a burr hole into lateral ventricle and foramen of Monro. The colloid cyst sits within the foramen of Monro and can be accessed through the lateral ventricle.

Fig. 8:

(Left) The brain tissue silicone mold is poured with the ventricles assembled using the square rods, and the foramen/cyst cavity already pre-cast out of stiffer silicone. (Right) Cyst preparation: the stretched Parafilm is placed over a tube and a syringe is filled with dilute agarose gel mixture.

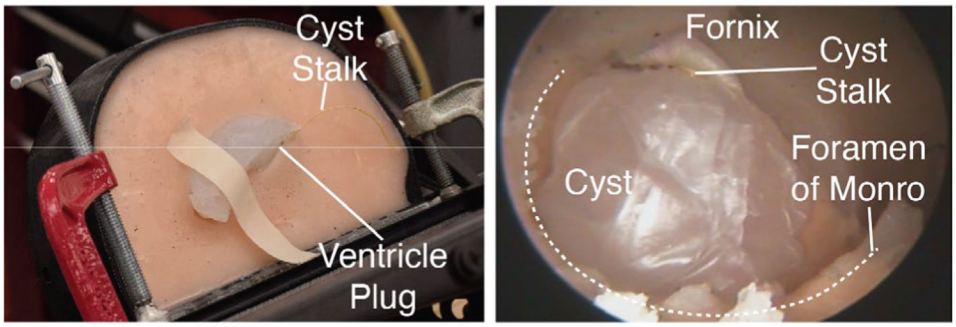

Fig. 9:

(Left) The phantom setup. The mating ventricle plug is shown, and the “stalk” of the cyst (the string) can also be seen. (Right) An endoscopic view of the anatomical layout for the phantom experiment. The foramen of Monro and fornix are cast from silicone, as is the rest of the brain phantom, while the cyst is made from a combination of stretched parafilm and a viscous agarose fluid/gel.

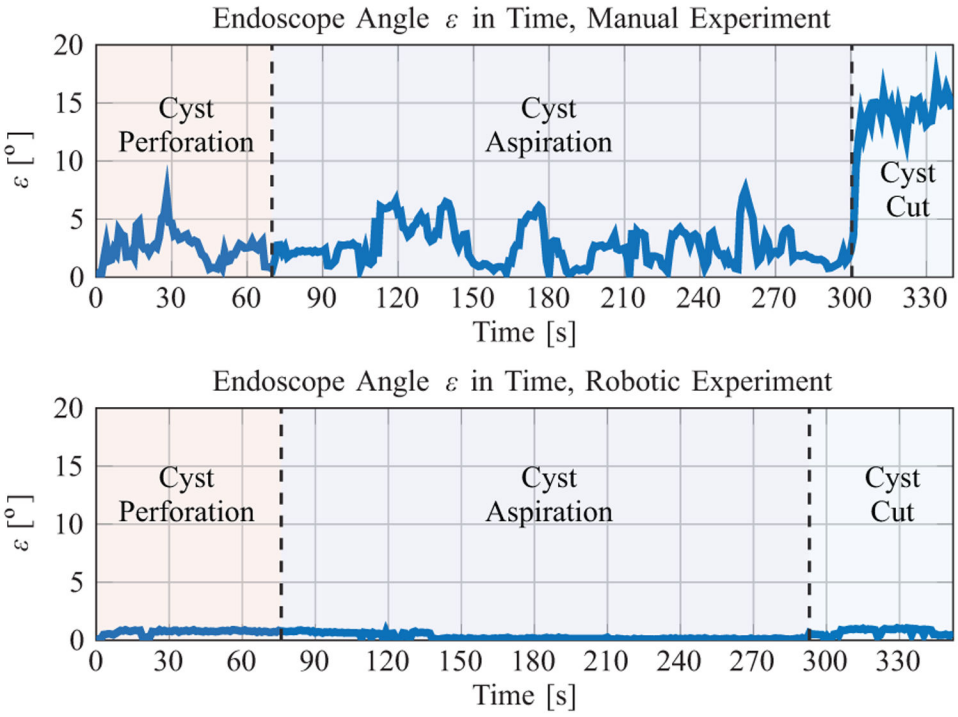

Fig. 10:

The endoscope angle in time for the manual (Top) and robotic (Bottom) phantom colloid cyst removal experiment.

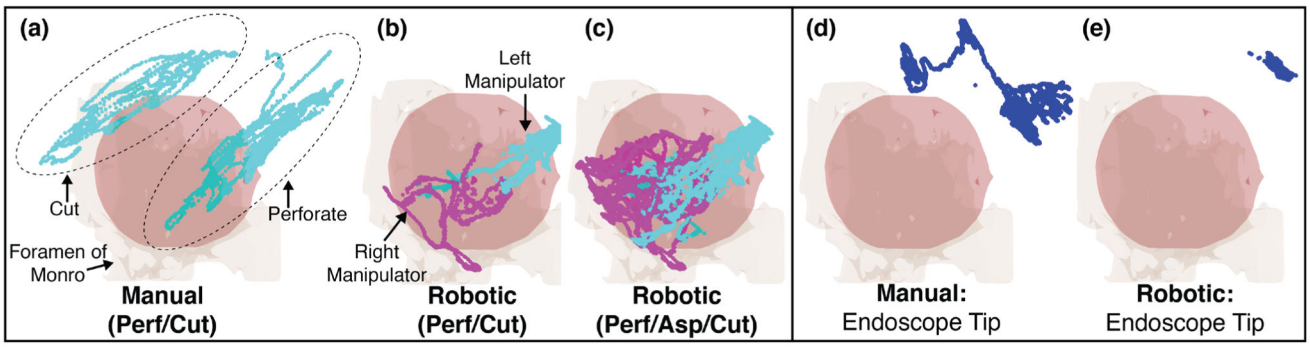

Fig. 11:

(a)-(c) Manual and robotic tool tip positions for the experiments. During the manual experiment, aspiration was not tracked. In the robotic experiment, joint positions of both arms were recorded for the entire duration. (d)-(e) Endoscope tip positions for both the manual and robotic experiments.

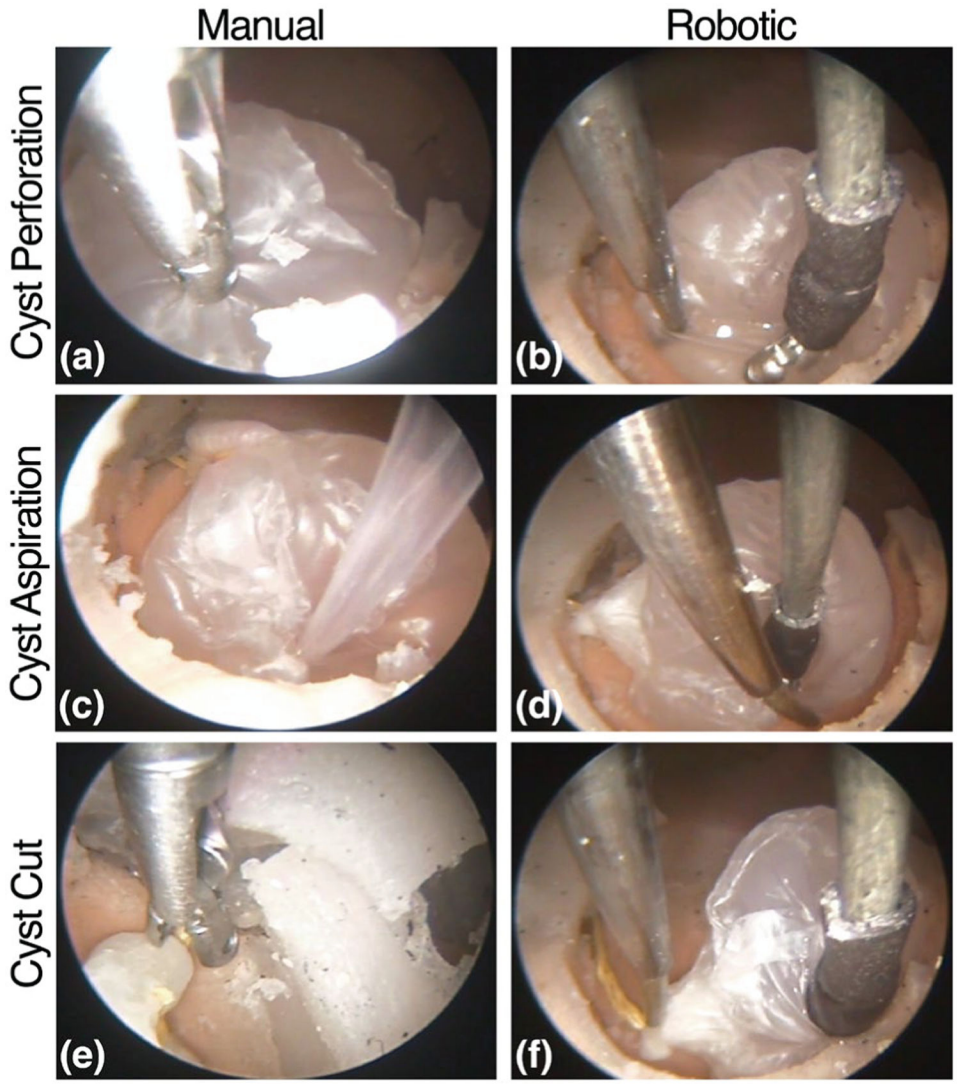

Fig. 12:

(a) The cyst is perforated by grabbing the membrane and pulling/twisting. (b) The left and right arm provide tension to open the cyst. (c) The cyst is poked with the aspiration tube until it is debulked. (d) The right arm is used to move the cyst off of the floor so that the left arm can aspirate the cyst contents beneath it. (e) The entire endoscope is moved substantially (see Fig. 10 - Top, and notice the shifted endoscopic view) so that the forceps can grasp the string. (f) The right arm moves the cyst towards the left arm which reaches to touch the string.

TABLE I:

Dimensions for components of robotic system

Component	Dimension	Units
Endoscope OD	8.3	mm
Endoscope Working Channel (Elliptical)	6.3 x 3.7	mm
Inner Tube OD	1.2	mm
Inner Tube ID	1.0	mm
Inner Tube Precurvature	15	m^{-1}
Inner Tube Curved Length	30	mm
Outer Tube OD	1.7	mm
Outer Tube ID	1.4	mm
Outer Tube Precurvature	40	m^{-1}
Outer Tube Curved Length	11	mm
Robot Dimensions (W x H x L)	105 x 84 x 280	mm
Robot Weight	2.70	kg
Lead Screw Pitch	20	threads*in^{-1}
Threaded/Keyed Gear Teeth	40	teeth

TABLE II:

The endoscopic angulation ε in time for each of the two phantom experiments.

	Manual	Robotic	Units
Mean $\varepsilon(t)$	3.97	0.46	deg
Max $\varepsilon(t)$	17.09	1.16	deg
Standard Deviation $\varepsilon(t)$	3.95	0.33	deg
Experiment Time	340.6	353.0	S

TABLE III:

Tool motion data for both the manual and robotic experiments. The endoscope is tracked during both experiments. The 1D motion of the forceps is tracked during the manual procedure, and the positions of the manipulators are logged in software during the robotic procedure. For the manual procedure, these values include the forcep motions when the tool is inside of the endoscope.

	Manual Forceps	Robotic Left Arm	Robotic Right Arm	Units
Tip Distance: Perf	479	201	218	mm
Total Time: Perforation	70	76	76	s
Average Velocity: Perf	6.8	2.6	2.9	$mm/_s$
Tip Distance: Cut	354	230	267	mm
Total Time: Cut	40	60	60	s
Average Velocity: Cut	8.9	3.8	4.5	$mm/_s$